Fabrication of bowtie aperture antennas for producing sub-20 nm optical spots

Yang Chen,[1] Jianfeng Chen,[1] Xianfan Xu[2,3] and Jiaru Chu[1,4]

[1]*Department of Precision Machinery and Precision Instrumentation, University of Science and Technology of China, Hefei 230026, China*
[2]*School of Mechanical Engineering and Birck Nanotechnology Center, Purdue University, West Lafayette, Indiana 47907, USA*
[3]*xxu@purdue.edu*
[4]*jrchu@ustc.edu.cn*

Abstract: Bowtie aperture antennas are known to generate sub-diffraction limited optical spots in the visible and near-infrared frequencies, which can be applied to many areas. Regular bowtie apertures fabricated by FIB suffer from tapered sidewall and rounded corner, which degrade its optical enhancement and localization. In this work, a new fabrication method is demonstrated to manufacture bowtie aperture antennas which can produce optical spots with lateral size smaller than 20 nm. We also employ numerical simulations to compute the near-field distribution on the surface of the bowtie aperture with topography extracted from the fabrication antennas. The near-field distribution measured by s-NSOM agrees well with the simulation and confirms the improved near-field localization of our bowtie aperture. This new fabrication method can be applied to other types of ridged apertures, which promises wide applications of deep sub-diffraction limited optical spots in many areas.

©2015 Optical Society of America

OCIS codes: (220.4241) Nanostructure fabrication; (310.6628) Subwavelength structures, nanostructures.

References and links

1. S. Kim, H. Jung, Y. Kim, J. Jang, and J. W. Hahn, "Resolution limit in plasmonic lithography for practical applications beyond 2x-nm half pitch," Adv. Mater. **24**(44), OP337–OP344 (2012).
2. L. Wang, S. M. Uppuluri, E. X. Jin, and X. Xu, "Nanolithography using high transmission nanoscale bowtie apertures," Nano Lett. **6**(3), 361–364 (2006).
3. L. Wang and X. Xu, "High transmission nanoscale bowtie-shaped aperture probe for near-field optical imaging," Appl. Phys. Lett. **90**(26), 261105 (2007).
4. S. Park, J. W. Hahn, and J. Y. Lee, "Doubly resonant metallic nanostructure for high conversion efficiency of second harmonic generation," Opt. Express **20**(5), 4856–4870 (2012).
5. M. Mivelle, T. S. van Zanten, L. Neumann, N. F. van Hulst, and M. F. Garcia-Parajo, "Ultrabright bowtie nanoaperture antenna probes studied by single molecule fluorescence," Nano Lett. **12**(11), 5972–5978 (2012).
6. J. Berthelot, S. S. Aćimović, M. L. Juan, M. P. Kreuzer, J. Renger, and R. Quidant, "Three-dimensional manipulation with scanning near-field optical nanotweezers," Nat. Nanotechnol. **9**(4), 295–299 (2014).
7. B. C. Stipe, T. C. Strand, C. C. Poon, H. Balamane, T. D. Boone, J. A. Katine, J.-L. Li, V. Rawat, H. Nemoto, A. Hirotsune, O. Hellwig, R. Ruiz, E. Dobisz, D. S. Kercher, N. Robertson, T. R. Albrecht, and B. D. Terris, "Magnetic recording at 1.5 Pb m−2 using an integrated plasmonic antenna," Nat. Photonics **4**(7), 484–488 (2010).
8. K. Şendur, C. Peng, and W. Challener, "Near-field radiation from a ridge waveguide transducer in the vicinity of a solid immersion lens," Phys. Rev. Lett. **94**(4), 043901 (2005).
9. C. Peng, E. X. Jin, T. W. Clinton, and M. A. Seigler, "Cutoff wavelength of ridge waveguide near field transducer for disk data storage," Opt. Express **16**(20), 16043–16051 (2008).
10. C. Genet and T. W. Ebbesen, "Light in tiny holes," Nature **445**(7123), 39–46 (2007).
11. A. V. Itagi, D. D. Stancil, J. A. Bain, and T. E. Schlesinger, "Ridge waveguide as a near-field optical source," Appl. Phys. Lett. **83**(22), 4474 (2003).
12. X. Shi, L. Hesselink, and R. L. Thornton, "Ultrahigh light transmission through a C-shaped nanoaperture," Opt. Lett. **28**(15), 1320–1322 (2003).

#233732 - $15.00 USD Received 3 Feb 2015; revised 23 Mar 2015; accepted 23 Mar 2015; published 1 Apr 2015

13. F. Chen, A. Itagi, J. A. Bain, D. D. Stancil, T. E. Schlesinger, L. Stebounova, G. C. Walker, and B. B. Akhremitchev, "Imaging of optical field confinement in ridge waveguides fabricated on very-small-aperture laser," Appl. Phys. Lett. **83**(16), 3245 (2003).
14. E. X. Jin and X. Xu, "Obtaining super resolution light spot using surface plasmon assisted sharp ridge nanoaperture," Appl. Phys. Lett. **86**(11), 111106 (2005).
15. I. A. Ibrahim, M. Mivelle, T. Grosjean, J. T. Allegre, G. W. Burr, and F. I. Baida, "Bowtie-shaped nanoaperture: a modal study," Opt. Lett. **35**(14), 2448–2450 (2010).
16. M. Y. Ali, W. Hung, and Y. Q. Fu, "A review of focused ion beam sputtering," International Journal of Precision Engineering and Manufacturing. **11**(1), 157–170 (2010).
17. L. Frey, C. Lehrer, and H. Ryssel, "Nanoscale effects in focused ion beam processing," Appl. Phys., A Mater. Sci. Process. **76**(7), 1017–1023 (2003).
18. T. Ishitani, K. Umemura, T. Ohnishi, T. Yaguchi, and T. Kamino, "Improvements in performance of focused ion beam cross-sectioning: aspects of ion-sample interaction," J. Electron Microsc. (Tokyo) **53**(5), 443–449 (2004).
19. A. Lugstein, B. Basnar, J. Smoliner, and E. Bertagnolli, "FIB processing of silicon in the nanoscale regime," Appl. Phys., A Mater. Sci. Process. **76**(4), 545–548 (2003).
20. J. Melngailis, "Focused ion beam technology and applications," J. Vac. Sci. Technol. B **5**(2), 469 (1987).
21. J. Zhang, M. Irannejad, and B. Cui, "Bowtie nanoantenna with single-digit nanometer gap for Surface-enhanced raman scattering (SERS)," Plasmonics 10.1007/s11468-014-9870-5 (2014).
22. H. Kollmann, X. Piao, M. Esmann, S. F. Becker, D. Hou, C. Huynh, L. O. Kautschor, G. Bösker, H. Vieker, A. Beyer, A. Gölzhäuser, N. Park, R. Vogelgesang, M. Silies, and C. Lienau, "Toward plasmonics with nanometer precision: nonlinear optics of helium-ion milled gold nanoantennas," Nano Lett. **14**(8), 4778–4784 (2014).
23. E. D. Palik, *Handbook of Optical Constants of Solids* (Academic, 1998).
24. T. Søndergaard, S. I. Bozhevolnyi, S. M. Novikov, J. Beermann, E. Devaux, and T. W. Ebbesen, "Extraordinary optical transmission enhanced by nanofocusing," Nano Lett. **10**(8), 3123–3128 (2010).
25. M. Schnell, A. Garcia-Etxarri, J. Alkorta, J. Aizpurua, and R. Hillenbrand, "Phase-resolved mapping of the near-field vector and polarization state in nanoscale antenna gaps," Nano Lett. **10**(9), 3524–3528 (2010).
26. R. Hillenbrand and F. Keilmann, "Complex optical constants on a subwavelength scale," Phys. Rev. Lett. **85**(14), 3029–3032 (2000).
27. N. Ocelic, A. Huber, and R. Hillenbrand, "Pseudoheterodyne detection for background-free near-field spectroscopy," Appl. Phys. Lett. **89**(10), 101124 (2006).
28. R. Esteban, R. Vogelgesang, and K. Kern, "Tip-substrate interaction in optical near-field microscopy," Phys. Rev. B **75**(19), 195410 (2007).
29. R. L. Olmon, M. Rang, P. M. Krenz, B. A. Lail, L. V. Saraf, G. D. Boreman, and M. B. Raschke, "Determination of electric-field, magnetic-field, and electric-current distributions of infrared optical antennas: a near-field optical vector network analyzer," Phys. Rev. Lett. **105**(16), 167403 (2010).
30. M. B. Raschke and C. Lienau, "Apertureless near-field optical microscopy: Tip–sample coupling in elastic light scattering," Appl. Phys. Lett. **83**(24), 5089 (2003).
31. N. Zhou, Y. Li, and X. Xu, "Resolving near-field from high order signals of scattering near-field scanning optical microscopy," Opt. Express **22**(15), 18715–18723 (2014).

1. Introduction

Plasmonic devices made of ridged aperture antennas have been applied to areas such as near-field lithography [1, 2], near-field microscopy [3], nonlinear optics [4, 5], nano-manipulation [6] and high-density data storage [7–9], for its ability to achieve extraordinary transmission and produce sub-diffraction-limited enhanced optical spot in the visible and near-infrared frequencies [10, 11]. In these applications, the excitation laser is incident from one side of the aperture, i.e., the entrance side, transmitted by the aperture, and then radiated into the other side, i.e., the exit side as a localized near-field light spot. For the ridged apertures mainly in C [12, 13], I, H and bowtie [14, 15] shapes, the lateral gap size on the exit side is a critical parameter. Smaller gap size leads to more intense and more confined near-field spot and is preferred in the applications mentioned above.

Usually, focused ion beam (FIB) is used to directly fabricate ridged apertures in a thin film of metal. Despite its advantage of nanoscale resolution, material insensitivity and process simplicity, focused ion beam milling suffers from one serious problem: non-vertical sidewall with taper and rounded corner [16]. The taper results from the combined effects of Gaussian ion beam profile, angle-dependent sputtering yield of incident ion, and redeposition. The rounded corner is mainly caused by the non-Gaussian tail of the ion beam [17]. Owing to this problem, the lateral gap size at the exit side is apparently enlarged even though the gap at the entrance side can be very small. As a result, the optical performance is degraded. Some research has been conducted to reduce sidewall taper and fabricate high aspect ratio structure

[18, 19]. But up to date, fabrication of ridged aperture with gap size below 20 nm is still a challenge.

In this work, we report a new fabrication method which can manufacture bowtie aperture with a sub-20 nm gap. Bowtie aperture is fabricated on a gold film coated on a suspended silicon nitride membrane using focused ion beam (FEI Helios Nanolab 650) milling. During application, light will be delivered from the side of the silicon nitride membrane and exit through the aperture at the surface of the gold film, which is made small. We use the finite difference time domain (FDTD) method to simulate the near-field performance of the fabricated bowtie aperture based on its actual topography. The near-field distribution is then measured using scattering-type near-field scanning optical microscopy (s-NSOM) and compared with the simulated results. It is concluded that the bowtie aperture fabricated by this new method can produce an optical spot as small as 20 nm in lateral size.

2. Fabrication

The fabrication process is described in Fig. 1. A SiO_2 film (thickness: 2 µm) and a Si_3N_4 film (thickness: 300 nm) are deposited respectively on the two sides of the Si wafer (thickness: 300 µm). Then a window of 1 mm × 1 mm is patterned by photo lithography, and the SiO_2 film in the window is removed by Reactive Ion Etching (RIE, CHF_3:Ar = 1:1). After that, the bulk Si in the window is removed by Inductively Coupled Plasma etching (ICP) and KOH wet etching. Then a gold film (thickness: 80 nm) is deposited on the Si_3N_4 film by E-beam evaporation. In the following step, we thin the Si_3N_4 layer to about 50 nm at the center of the window using large current FIB milling (30KV, 9.3nA). Thinner Si_3N_4 is favorable in time saving and accurate dose control in the next step of bowtie aperture fabrication, because the milling rate of Si_3N_4 is much slower than Au. On the other hand, it is difficult to etch out the Si_3N_4 layer without removing part of the Au. Thus about a 50 nm-thick Si_3N_4 membrane is retained, which can also protect the surface of Au film from Ga^+ ion implantation in the following step [20]. Lastly we perforate bowtie apertures on the thinned Si_3N_4 membrane using FIB (30KV, 7.7pA). Accurate dose control in the gap area is critical: insufficient dose causes incomplete material remove and over dose enlarges the gap size. In our fabrication, the dwell time of ion beam on a single pixel is set to 1 µs, and the scan passes on the whole aperture except the corner is set to 615. In the corner, the scan passes is tripled for serious redeposition there.

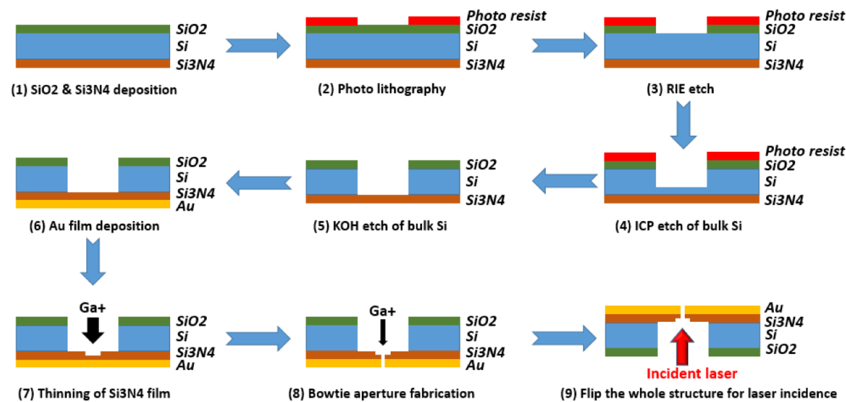

Fig. 1. Schematic of the fabrication process.

The bowtie apertures fabricated using the procedures described above will have the incident light from the Si_3N_4 membrane side. The top surface of the gold film is used as the exit plane of light. An example of the fabricated bowtie aperture is shown in Fig. 2. Its lateral gap size on the exit side is 16 nm. By fabricating and measuring dozens of bowtie apertures,

the gap size on the exit side is controlled consistently below 20 nm, and the smallest one is less than 10 nm. Electron Beam Lithography (EBL) [21] and milling-based He^+-ion lithography (HIL) [22] can also be used to fabricate gap antennas with gap size below 10 nm. But it's difficult for EBL to fabricate structures with high-aspect-ratio and achieve 20 nm gap in bowtie aperture with 80 nm thickness. As to HIL, it's indeed the state-of-the-art fabrication method but not as popular as Ga^+-FIB around the world. Also its milling speed is much slower than Ga^+-FIB.

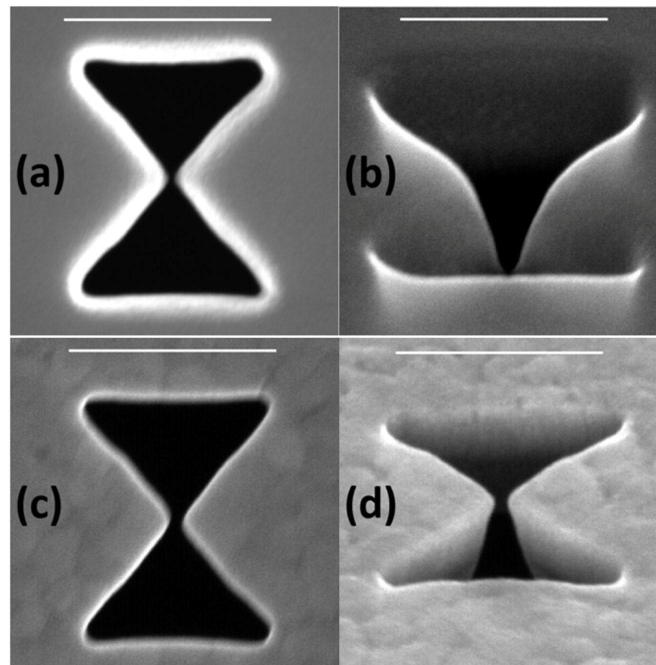

Fig. 2. SEM images of one fabricated bowtie aperture (scale bar: 300nm). (a), (b) top view and side view (52deg with respect to the normal of the sample) on Si_3N_4 side, (c), (d) top view and side view on Au side.

3. Numerical simulations

To simulate the near-field distribution of the bowtie aperture at the wavelength of 633 nm, we use commercial finite difference time domain software (Lumerical FDTD Solutions). Optical properties of Si_3N_4 and Au are taken from [23]. The topography parameters of the aperture are extracted from the SEM pictures. The radius of curvature in the center and at the corner are set 10 nm and 5 nm. By measuring and averaging several bowtie apertures, we set the taper angle θ as 78 deg. The rounded corner only exists in Si_3N_4 layer and have minimal effect on the optical performance. The total-field scattered field (TFSF) source is used with amplitude of 1 V/m and the polarization is set to be across the gap shown in Fig. 3(b). Frequency-domain field profile monitor is set 2 nm above the exit plane. To simulate the taper topography accurately, 1 nm × 1 nm × 1 nm mesh size is used in the aperture area.

#233732 - $15.00 USD Received 3 Feb 2015; revised 23 Mar 2015; accepted 23 Mar 2015; published 1 Apr 2015
© 2015 OSA

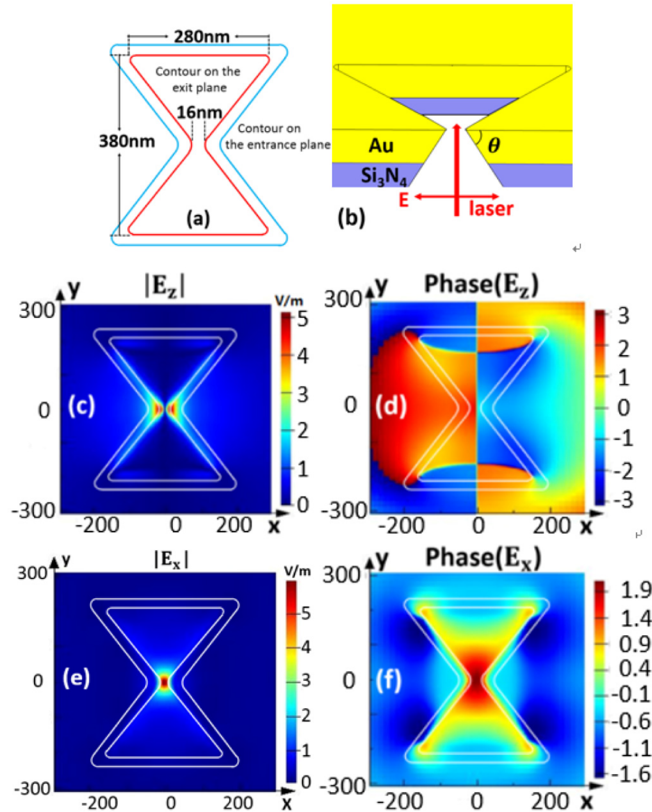

Fig. 3. (a), (b) schematic of the simulation model. (c)- (f) FDTD simulation results in a 600 × 600 nm^2 region. (c), (d) amplitude and phase of E_z, (e), (f) amplitude and phase of E_x.

Figures 3(c)-3(f) show the simulated near-field distribution. For the E_x component, one single enhanced spot is localized in the gap, with continuous phase across the gap. For the E_z component, two enhanced spots are localized on each side of the gap, with 180° phase shift across the gap. We compare enhancement and localization of a bowtie aperture fabricated using our method, a bowtie aperture with perfect side wall and a regular bowtie aperture in Table 1. By perfect side wall, we mean the side wall with no taper and no rounded corner, and the aperture shape on the exit plane is the same as the aperture fabricated in this work. The regular aperture refers to the aperture milled from the gold side, i.e., the taper and rounded corners shown in the silicon nitride film now appear on the gold film, and the light radiates from the silicon nitride side. In Table 1, width of E_x means FWHM of the single peak of E_x and width of E_z means the distance between two peaks of E_z. Both of them are used to describe the near-field localization of bowtie aperture.

Table 1. Near-field localization and enhancement of three types of bowtie apertures

	Peak amplitude of E_x (V/m)	Peak amplitude of E_z (V/m)	Gap width on the exit plane(nm)	Width of E_x (nm)	Width of E_z (nm)
Aperture with perfect side walls	14.95	20.19	16	17	16
Aperture made in this work	19.83	23.81	16	17	16
Regular aperture with tapered walls	4.96	7.17	49	51	50

From Table 1, we can see that relative to the aperture with perfect side wall, the bowtie aperture fabricated in our method has similar performance in near-field localization and better performance in near-field enhancement, and the regular aperture is degraded in both aspects. The size of the near-field spot is mainly determined by the gap size on the exit side. As to the enhanced field amplitude of our bowtie aperture, it is likely due to the fact that the larger aperture on the entrance plane collects more incident light [24].

4. s-NSOM measurement

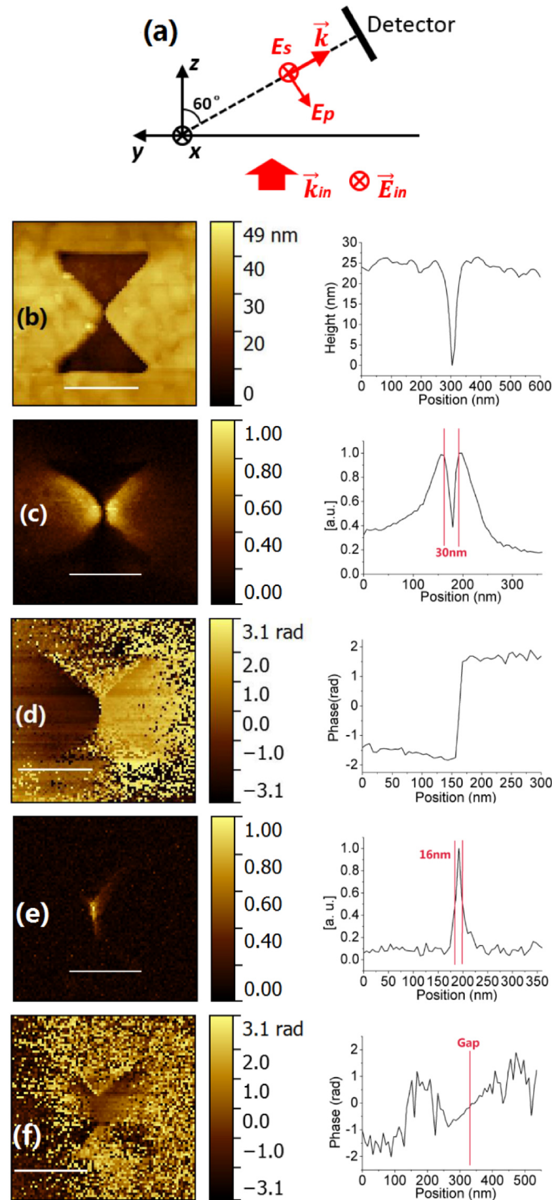

Fig. 4. s-NSOM results, scan range: 500 nm × 500 nm, scan bar: 200 nm. The amplitude signal is normalized. (a) Schematic of the collection path and far field polarizations. (b) Topography. (c), (d) Amplitude and phase of E_p. (e), (f) Amplitude and phase of E_s. The pictures of the right column are cutline curves across the gap of the bowtie aperture in the pictures of the left column.

#233732 - $15.00 USD Received 3 Feb 2015; revised 23 Mar 2015; accepted 23 Mar 2015; published 1 Apr 2015
© 2015 OSA

To measure the near-field distribution of the bowtie aperture fabricated in this work, we use a commercial scattering-type near-field scanning optical microscope (s-NSOM, from Neaspec GmbH) in the transmission mode [25]. The system is based on an AFM working in the tapping mode. A 633 nm HeNe laser is incident upward on the sample with polarization across the bowtie gap as the excitation source. The light scattered by the tip is collected and directed to a photodetector. Higher harmonics demodulation [26] and pseudoheterodyne detection [27] is used to extract and amplify the near-field signal from background. The tip we use is a commercial Si AFM probe (ARROW-NCR, NanoWorld) to avoid plasmonic coupling between the tip and the sample [28]. The radius of the tip apex is 10 nm and the oscillation amplitude is 40 nm in our experiments. By adjusting the halfwave plate in the interference path and the polarizer in front of the photodetector, we can get near-field distributions of two orthogonal components E_p and E_s, which correspond to E_z and E_x of bowtie aperture in Fig. 3. The direction of the two pairs of vectors is shown in Fig. 4(a), and they can be mutually transferred by getting the scattering matrix of the tip [25, 29]. In our measurement, we first approach the tip to the surface of the Au film, then turn down the feedback of the AFM and scan the sample. Turning on the feedback of the AFM can make the tip penetrate deeply into the aperture and the near-field signal obtained is not the signal at the surface plane.

The topography of the bowtie aperture shown in Fig. 4(b) is obtained with AFM feedback turned on, which is slightly different from the SEM image because of the effect of AFM tip. The s-NSOM results are obtained at the 3rd harmonics of the oscillation frequency of the AFM tip, as shown in Figs. 4(c)-4(f). For the E_p component, we observe two adjacent hotspots on each side of the gap. The distance between the two peaks is 30 nm, and the FWHM of each peak is 80 nm. Inside the gap, the amplitude signal is very low, but a phase jump of about 180° is observed which agrees with the simulation result shown in Figs. 3(c) and 3(d). The phase signal cannot be demodulated and appears noisy in the area where the field amplitude is weak. For the E_s component, only one intense hotspot with FWHM of 16 nm is observed and localized in the gap, and the phase signal is continuous across the gap, which also agrees with the simulation results in Figs. 3(e) and 3(f). The size of the E_p and E_s components are slightly different from the simulation, because the resolution of s-NSOM is restricted by the radius of curvature of the tip [30], which is 10 nm in our case. In spite of this, the measured spot size is still much smaller than the previous results measured on the regular bowtie aperture [31].

5. Conclusions

In summary, the bowtie aperture manufactured using our method can produce optical spot with lateral size below 20 nm, which is demonstrated by FDTD simulation and s-NSOM measurement. By optimizing the fabrication parameters, our method has the potential to reduce the lateral spot size further. In addition, this method can be applied to the fabrication of other types of ridged apertures to achieve better enhancement and localization. The ridged apertures fabricated by this method promise wide applications in many areas where deep sub-diffraction limited optical spots are needed.

Acknowledgments

This work is supported by the National Basic Research Program of China (973 Program, No.2011CB302101). Fabrication and s-NSOM measurement of the bowtie aperture are carried out in the USTC Center for Micro- and Nanoscale Research and Fabrication. X. Xu acknowledges the support from the US National Science Foundation.

#233732 - $15.00 USD Received 3 Feb 2015; revised 23 Mar 2015; accepted 23 Mar 2015; published 1 Apr 2015
© 2015 OSA